THE JOURNAL OF PHYSICAL CHEMISTRY B

Article

pubs.acs.org/JPCB

Computational and Experimental Characterizations of Silver Nanoparticle–Apolipoprotein Biocorona

Rongzhong Li,[†] Ran Chen,[§] Pengyu Chen,[§] Yimei Wen,[§] Pu Chun Ke,*[,§] and Samuel S. Cho*[,†,‡]

[†]Department of Physics, Wake Forest University, Winston-Salem, North Carolina 27106, United States

[‡]Department of Computer Science, Wake Forest University, Winston-Salem, North Carolina 27106, United States

[§]Department of Physics and Astronomy, Clemson University, Clemson, South Carolina 29634, United States

ABSTRACT: With the advancement of nanotoxicology and nanomedicine, it has been realized that nanoparticles (NPs) interact readily with biomolecular species and other chemical and organic matter to result in biocorona formation. The field of the environmental health and safety of nanotechnology, or NanoEHS, is currently lacking significant molecular-resolution data, and we set out to characterize biocorona formation through electron microscopy imaging and circular dichroism spectroscopy that inspired a novel approach for molecular dynamics (MD) simulations of protein–NP interactions. In our present study, we developed a novel GPU-optimized coarse-grained MD simulation methodology for the study of biocorona formation, a first in the field. Specifically, we performed MD simulations of a spherical, negatively charged citrate-covered silver nanoparticle (AgNP) interacting with 15 apolipoproteins. At low ion concentrations, we observed the formation of an AgNP–apolipoprotein biocorona. Consistent with the circular dichroism (CD) spectra, we observed a decrease in α-helices coupled with an increase in β-sheets in apolipoprotein upon biocorona formation.

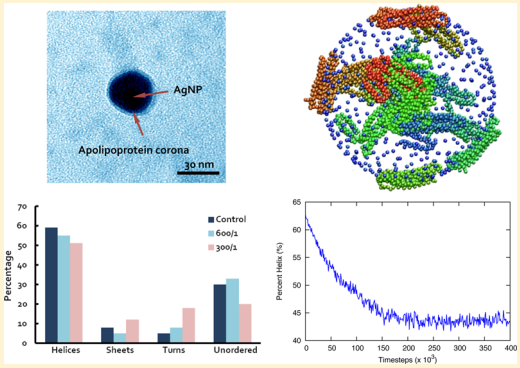

INTRODUCTION

The advent of nanoparticle systems has opened up many new exciting developments in biomedicine and technology.[1] Owing to their small size, large surface area-to-volume ratio, and versatile physicochemical properties, nanoparticles readily enter cells and organelles, leading to the possibilities of new medicine (nanomedicine) or biological hazard (nanotoxicity).[1,2] A key concept emerging in the fields of nanomedicine and nanotoxicity is the idea of protein–nanoparticle interactions that result in a dynamic layer of proteins and other biomolecules, or "corona",[2,3] that adsorbed onto a nanoparticle surface. In this view, nanoparticles entering any biological fluid will be covered by a corona of biomolecules with the latter to render the biological identity for the nanoparticle when interacting with the cellular machinery.[3] Although previous research has focused on the biomolecular composition of the corona and its composition evolution over time at a microscopic scale,[4−6] it is becoming apparent that protein interactions with a nanoscaled surface can disrupt the native conformation and therefore compromise the function of the protein. Furthermore, it has recently become an active area of inquiry as to how the entirety of nanoparticle–protein corona may evoke signaling and immune responses from the cell and be preserved and weathered upon cell uptake, cellular distribution, and discharge.[7,8] These questions can be addressed only with an adequate knowledge of the molecular details of nanoparticle–biocorona formation.

It is now well established that proteins and RNA fold into a well-defined conformation in order to carry out its biological function(s).[9] These biomolecules have been evolutionarily selected to minimize frustrated interactions[10,11] such that the folding and assembly energy landscape is funneled toward its native conformation.[12−16] A molecular dynamics approach that exploits the funneled energy landscape theory is a native structure-based Go-type Hamiltonian where there exists a global attractor to the native folded state,[17−19] and it has accurately characterized in vitro observables in both proteins[14,17,20,21] and RNA.[22−25] In a cellular in vivo medium, repulsive crowding effects can also be significant such that the folded state can be stabilized due to a reduction of entropy.[26] In contrast, interactions of a nanoparticle with proteins and other biomolecules may be attractive to enable adsorption of the biomolecules onto the nanoparticle surface, as is observed in molecular dynamics (MD) simulations of peptide aggregation on surfaces.[27,28]

While studies of protein adsorption to nanoparticles are becoming appreciated, the detailed molecular-resolution structure of the adsorbed protein–nanoparticle interface has only recently started being unravelled. In a recent coarse-grained MD simulation approach, protein–nanoparticle interactions were modeled where the proteins were represented as

Received: June 20, 2013
Revised: September 26, 2013
Published: September 27, 2013

rigid spheres or ellipsoids to study protein adsorption onto a surface.[29] Previous protein adsorption studies of bovine serum albumin (BSA), myoglobin (MB), and cytochrome c onto self-assembled monolayers of mercaptoundecanoic acid on Au nanoparticles showed that all three proteins formed adsorption layers consisting of an irreversibly adsorbed and a reversibly adsorbed fraction.

In this study, we focus on the interactions of a silver nanoparticle with apolipoprotein A-1, which is the main component of high-density lipoprotein (HDL), a heterogeneous mixture of lipoprotein particles. In blood, the apolipoprotein A-I recruits phospholipids and chloresterol to form discoidal HDL particles that mature into larger, spherical HDL particles.[30] Lipoprotein complexes are involved in the general cellular processes of cholesterol metabolism, and there are multiple receptors for apolipoprotein complexes at cell surfaces that nanoparticles can potentially exploit to enter cells.[31]

To characterize biocorona formation from joint computational and experimental approaches, we present a novel graphics-processing unit (GPU)-optimized coarse-grained Go-type MD simulation approach for protein−nanoparticle interactions at a molecular resolution that was inspired by and compared with a combination of TEM imaging and circular dichroism (CD) spectra measurements. The coarse-grained Go-type protein folding Hamiltonian that we used to model apolipoprotein was based on the well-established Funneled Energy Landscape Theory. To introduce nanoparticle−protein interactions, we employed the Debye−Hückel potential for ion concentration-dependent charge interactions between citrate-coated AgNPs and the charged apolipoprotein. We probed the secondary structural changes of apolipoprotein upon its binding to the AgNP, and we make direct quantitative comparisons of our simulations with experimentally measured CD spectra.

MATERIALS AND CHARACTERIZATION

AgNPs (30 nm in nominal diameter, citrate coating, "Biopure", Nanocompsix) and human apolipoprotein A-I (MW = 28.3 KDa, Sigma-Aldrich) of different concentrations were prepared by diluting the stock suspensions with Milli-Q water. The hydrodynamic sizes of the AgNPs (0.5 nM) and the apolipoprotein (150 and 300 nM) were obtained from dilutions of the stocks using dynamic light scattering (ZetaSizer Nano S90, Malvern Instruments). The zeta-potentials of the AgNPs (0.5 nM), the apolipoprotein (150 and 300 nM), and their mixtures of AgNP/apolipoprotein at molar ratios of 1:300 and 1:600 were measured using a ZetaSizer ZS (Malvern Instruments).

Transmission Electron Microscopy (TEM). Images of the AgNPs were obtained using a 4800 transmission electron microscope. Suspensions of the AgNPs were placed onto a copper grid and dried in air for a few minutes before being placed into a TEM sample chamber. The formation of AgNP−apolipoprotein corona was directly observed (Hitachi H7600). AgNPs (0.5 nM) were incubated with apolipoprotein (150 nM) at 4 °C overnight and negatively stained with phosphotungstic acid for 45 min prior to imaging. A thin layer of optically less dense material, inferred to be the apolipoprotein, was clearly visible on the AgNP surfaces.

Circular Dichroism (CD) Spectroscopy. CD measurements were performed using a Jasco J-810 spectropolarimeter (Easton, MD) to determine changes in the secondary structures of apolipoprotein A-I resulting from their interactions with the AgNPs. Suspensions of AgNPs (0.33 nM) and apolipoprotein A-I (100 and 200 nM) were made in Milli-Q and were mixed at two different AgNP/apolipoprotein molar ratios of 1:300 and 1:600. These samples were incubated at 4 °C in a refrigerator for 8 h. The CD spectra of the samples were obtained at room temperature over a wavelength range of 200−300 nm using quartz cuvettes and were averaged over three scans taken at a speed of 50 nm/min. The background of the AgNP suspension (in Milli-Q) was subtracted.

The ellipticity value (θ, in mdeg) provided by the instrument was converted to standard unit of deg·cm^2/dmol ($[\theta]$) using equation $[\theta] = (\theta \times M_0)/(10000 \times C_{soln} \times L)$, where M_0 is the mean residue molecular weight (118 g/mol), C_{soln} is the apolipoprotein concentration in the suspension (in g/mL), and L is the path length through the buffer (1 cm). Comparing to the control sample of the protein, the spectra of AgNP−apolipoprotein revealed changes in the contents of alpha-helices, beta-sheets, and turns.

Native Structure Based Coarse-Grained Protein Folding Hamiltonian. To perform MD simulations of protein folding, we used the well-established native structure-based Go-type coarse-grained model. The detailed energy function and parameters for the Go-type model can be found elsewhere,[17,18,32] but we briefly discuss it here for clarity. In this simplified representation of proteins, a single bead centered at the C_α position represents each residue. The Go-type model Hamiltonian consists of short-range interactions for the bond (H_{bond}), angle (H_{angle}), and torsional potential ($H_{torsion}$), and their equilibrium position, angle, and torsion angle corresponds to the native state. In addition to the connectivity and rotational degrees of freedom, it also consists of long-range interactions for stabilizing the native structure (H_{NC}), where all native contact interactions are attractive and all other interactions are repulsive. The result is a Hamiltonian whose energy landscape is ideally biased toward the native attractor:

$$H_{total} = H_{short} + H_{long}$$
$$H_{short} = H_{bond} + H_{angle} + H_{torsion}$$
$$H_{long} = H_{NC}$$

In this representation, the protein secondary structures are largely stabilized by the torsional angles, while the tertiary structures are mostly stabilized by the long-range attractive native contact interactions that are described by a Lennard-Jones equation, and all other interactions are repulsive:

$$H_{NC} = \sum_{i,j}^{native} \left[\left(\frac{\sigma_{ij}^{nat}}{r_{ij}} \right)^{12} - 2 \left(\frac{\sigma_{ij}^{nat}}{r_{ij}} \right)^{6} \right] + \sum_{i,j}^{non\text{-}native} \left(\frac{\sigma^{non}}{r_{ij}} \right)^{12}$$

where σ_{ij}^{nat} is the distance between the centers of mass of two residues in the native state and σ_{ij}^{non} is 3.8 Å. The interactions between two residues are said to be native if the distance between their centers of mass is less than 8 Å.

To measure the conformational change of the apolipoprotein, we adopted the fraction of native contacts Q as an order parameter.[33] On the basis of this measure, multiple trajectories, each consisting of multiple folding and unfolding events, were collected and analyzed using the weighted histogram analysis method (WHAM)[34] to calculate the specific heat profile with respect to temperature. The secondary structure content was calculated using the backbone torsional angles. We designated a torsional angle between four consecutive residues to corre-

dx.doi.org/10.1021/jp4061158 | J. Phys. Chem. B 2013, 117, 13451−13456

spond to α-helical secondary structure if its value is between 45 and 60°. The residue interaction frequency was computed by calculating the frequency of an amino acid from apolipoprotein that is within the distance cutoff of 7 Å after 500,000 timesteps, which is when most of the apolipoproteins are bound to the AgNP.

All MD simulations were performed with code specifically optimized for GPUs to gain increases in performance,[35,36] but our simulation approach is general and is applicable for traditional computational approaches.

Novel Coarse-Grained Protein−Nanoparticle Hamiltonian. We modeled a large spherical citrate-coated AgNP as 500 individual charged spherical beads randomly distributed a distance of 10 nm from the center. Together, they constituted a spherical model of an AgNP consisting of a charged citrate coat. We then added 15 apolipoproteins to the simulation system by placing it randomly around the AgNP such that its position was 15 nm from the center. This ensured that the apolipoproteins were proximal to the AgNP but did not overlap with it.

With the initial positions of the apolipoprotein−AgNP complete, we then focused on the interactions between the two different simulation constituents. In addition to native contact interaction, each apolipoprotein and AgNP interaction consisted of two additional sets of interactions: (1) excluded volume and (2) electrostatic interactions:

$$H_{\text{long}} = H_{\text{NC}} + H_{\text{EV}} + H_{\text{elec}}$$

In this representation, each AgNP bead has excluded volume interactions with each apolipoprotein bead:

$$H_{\text{EV}} = \sum_{i,j}^{\text{protein}-\text{NP}} \left(\frac{\sigma}{r_{ij}}\right)^{12}$$

where r_{ij} is the distance between two interacting beads and σ is set to 3.8 Å.

Also, the negatively charged AgNP bead, which models a citrate-coated AgNP, has electrostatic interactions (H_{elec}) with the charged apolipoprotein residues. To maximize the biocorona formation, we only included electrostatic interactions involving positively charged residues. The electrostatic interactions between the protein and nanoparticle beads are represented by the Debye−Hückel potential:

$$H_{\text{elec}} = \sum_{i,j}^{\text{protein}-\text{NP}} \frac{z_i z_j e^2}{4\pi\epsilon_0\epsilon_r r} \, e^{-r/l_D}$$

The Debye length, l_D, is tuned to reflect the changes in ion-concentration, z is the charge between interacting beads, and r is the distance between them. Recent studies of protein and RNA folding coarse-grained MD simulations have shown remarkable agreement with experiments when supplementing the Go-type Hamiltonian with the Debye−Hückel potential.[23,37,38]

We performed Langevin MD simulations with a very low friction coefficient for more effective sampling of the free energy landscape.[39] For each MD simulation trajectory, we performed independent MD simulations at an ion concentration that corresponds to $[Na^+]$ = 0.020 M at a temperature of 300 K.

In all, the MD simulation protocol involves 15 apolipoproteins that each consists of 243 residues and 500 citrate-coated AgNP beads (with charge −1) that have computationally intensive electrostatic interactions with each of the basic residue beads (with charge +1). For this reason, we again performed all MD simulations code specifically optimized for GPUs to gain increases in performance,[35,36]

RESULTS AND DISCUSSION

The hydrodynamic size of the AgNPs was measured by DLS as 35.7 nm, while the hydrodynamic sizes of AgNP−lipoproprotein coronas were 38.5 and 39.4 nm for the NP/protein molar ratios of 1:300 and 1:600. In contrast, the hydrodynamic size of the apolipoprotein A-I was ∼1.9 nm. Accordingly, the zeta potentials of the AgNPs and apolipoprotein were determined to be −42.5 and −33.7 mV, while the zeta potentials of the AgNP−apolipoproperin mixtures were −37.4 and −38.6 mV for the NP/protein molar ratios of 1:300 and 1:600, respectively. The sizes of the AgNPs and AgNP−apolipoprotein coronas were determined by TEM as 30 and 34 nm, in agreement with the DLS size measurement. Since the protein layer is ∼2 nm from the TEM imaging and ∼3 nm from the DLS measurement, while the width of an α helix is ∼0.4 nm (Figure 2A), multilayer protein coating on the AgNPs was deemed plausible.

To characterize the biocorona formation of an AgNP interacting with apolipoprotein, we developed a novel coarse-grained MD simulation approach based on well-established models of protein folding. As a starting point, we characterized the protein folding behavior of apolipoprotein using a native structure based Go-type Hamiltonian. Apolipoprotein is an α-helical protein that consists of three helices (Figure 1A). The specific heat profile with respect to temperature shows that the folding mechanism consists of two distinct peaks that correspond to two melting temperatures (Figure 1B).

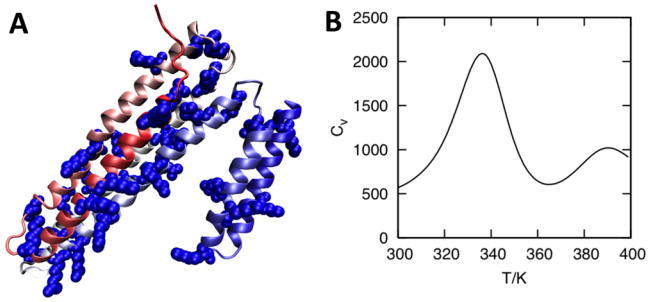

Figure 1. Folding of apolipoprotein A-I. (A) A ribbon diagram of a single apolipoprotein colored from the N-terminal (red) to C-terminal (blue) in a spectrum along its sequence. The positively charged basic residues are shown in a space-filled representation. (B) Specific heat profile with respect to temperature from coarse-grained Go-model folding simulations of a single apolipoprotein.

We then developed a coarse-grained MD simulation Hamiltonian for the biocorona formed from dehydrated citrate-coated AgNPs interacting with apolipoproteins. On the basis of the TEM observation (Figure 2A) and our knowledge about the chemical structure of the citrate that lines the AgNP, we expect that the major contributors to the protein−nanoparticle interactions would be expected to be excluded volume interactions and electrostatic interactions between the negatively charged citrate and the positively charged residues in apolipoprotein. As such, in our Hamiltonian, we introduced a charged, spherical AgNP that consisted of 500 individual charged spheres with excluded volume. We then added 15

dx.doi.org/10.1021/jp4061158 | J. Phys. Chem. B 2013, 117, 13451−13456

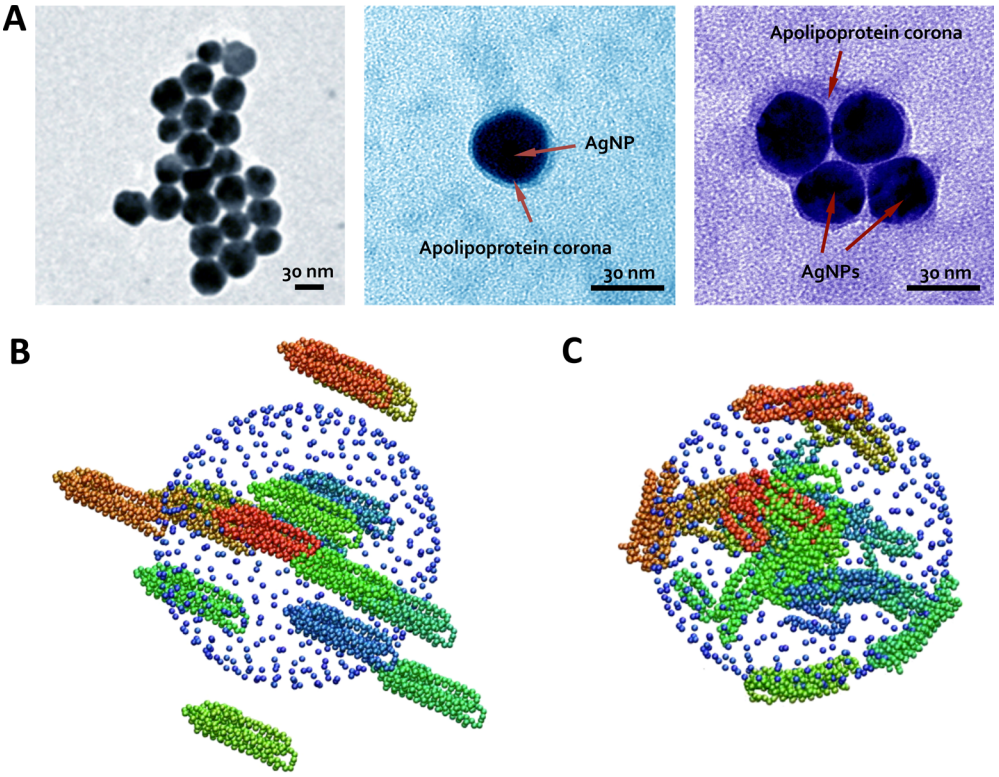

Figure 2. Biocorona formation from interactions of AgNPs with apolipoprotein A-I. (A) TEM images of (left) dehydrated citrate-coated AgNPs of 30 nm and (middle-right) AgNP–apolipoprotein coronas. (B) The initial setup of a coarse-grained MD simulation of 15 apolipoproteins (colored red, gray, and blue) near a negatively charged spherical model of AgNP (blue) that is 20 nm in diameter. (C) A snapshot of an AgNP–apolipoprotein biocorona from our GPU-optimized coarse-grained MD simulations at $[Na^+]$ = 0.020 M.

apolipoproteins in random positions proximal to the AgNP surface (Figure 2B).

Once the apolipoprotein–AgNP system was set up, we performed MD simulations of the system over a range of ion concentrations. In a relatively short period of time, the apolipoproteins became attracted to the AgNP and adhered to its surface (Figure 2C). We also performed CD spectra of apolipoprotein in the presence of AgNP at 300:1 and 600:1 concentrations of the protein. We observe decreases in α-helical content of the apolipoprotein in both cases (Figure 3A). To make a direct quantitative comparison with this observation, we monitored the secondary structure content in the MD simulation by measuring the backbone torsional angle of the apolipoprotein, and we observed a reduction in the α-helical content from about 65% to 45% (Figure 3B).

The conformational changes we observe in both our MD simulations and circular dichroism (CD) spectra are consistent with previous experimental studies. The interaction between human adult hemoglobin (Hb) and bare CdS quantum dots have been investigated by a number of techniques including CD spectroscopy. The CdS quantum dots decrease the α-helical content of the secondary structure from 72.5% to 60.5%.[40] Similar effects are observed with polystyrene nanoparticles that caused the α-helical content of BSA to reduce while the beta-turn fraction to increased.[41]

We next analyzed the per residue interaction frequency over the course of the MD simulation after 500,000 timesteps (Figure 3C) when the biocorona formation is largely complete because the proteins are proximal to the AgNP (Figure 3D). The positively charged residues, namely, arginine and lysine, are found to interact with the AgNP with greatest frequency as compared to the other residues present in the apolipoprotein. These are also the residues that have attractive electrostatic interactions with the negatively charged AgNP. Other effects, such as the hydrophobicity of the residues, do not seem to play a significant role in the interaction between the apolipoprotein and the AgNP in our present model. A recent kinetic modeling study of the corona complex formation process predicts two phases that involves a metastable state before reaching a stable state.[42] In our MD simulations, we only observe a single transition to a stable state (Figure 3D), but another might be observed if our simulations included a greater number of apolipoproteins at higher ion concentrations.

■ CONCLUSIONS

To characterize the biocorona formation, we carried out a joint computational and experimental study of AgNPs binding with apolipoprotein A-I. Specifically, we developed a new GPU-optimized coarse-grained MD simulation approach for biocorona formation and showed its consistencies with the experimental methodologies of DLS, TEM imaging, and CD spectroscopy. In both simulations and experiments, we observe a marked decrease in α-helical content of the protein as a result of their interactions with the AgNPs, in agreement with previous experimental studies on NP–protein corona. Our MD simulation approach is general and applicable to other biomolecule–nanoparticle systems, and it is amenable to increase in chemical detail. The effect of protein–protein interactions and nonelectrostatic residue specific interactions may also play important roles in biocorona formation that will be addressed in future work.

dx.doi.org/10.1021/jp4061158 | J. Phys. Chem. B 2013, 117, 13451–13456

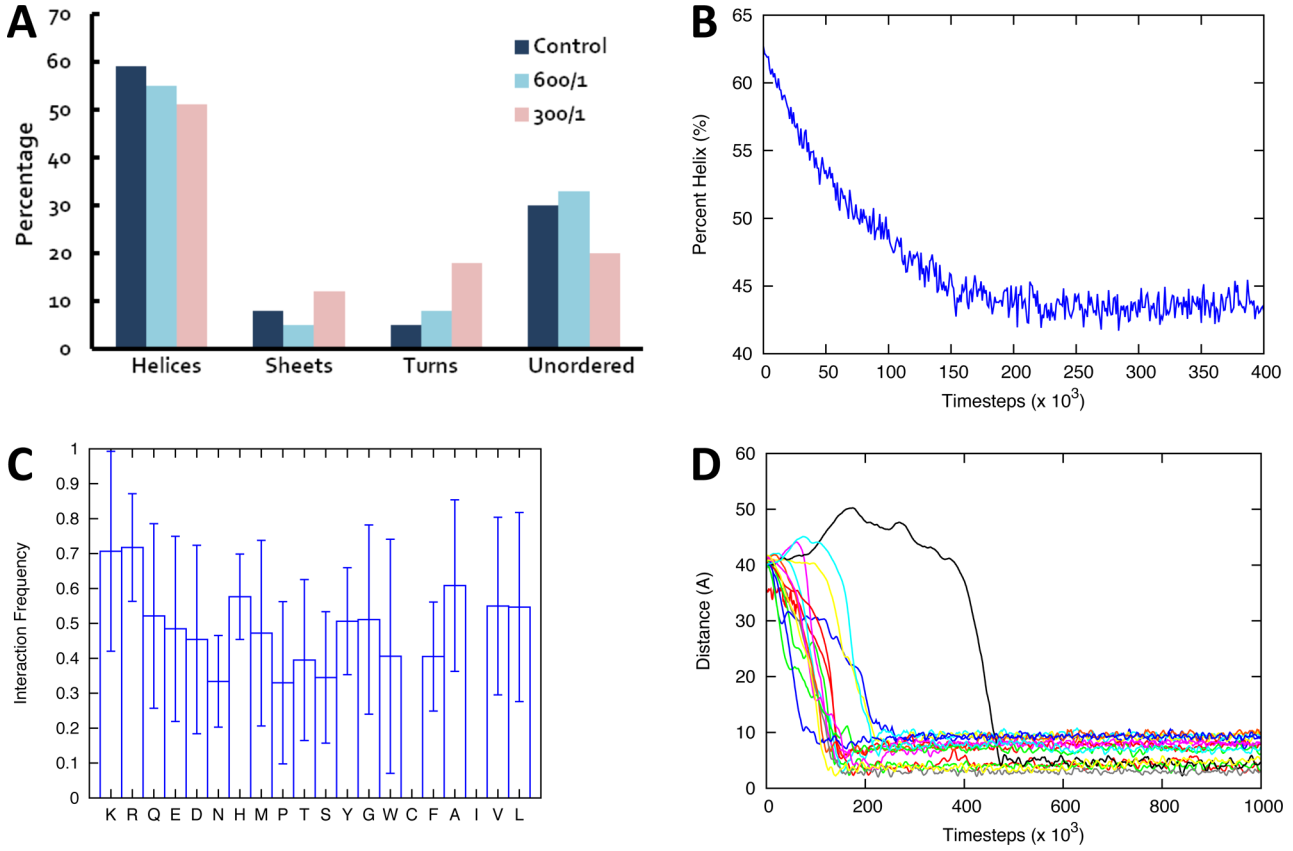

Figure 3. Reduction of α-helical content upon biocorona formation. (A) Secondary structure contents are shown for apolipoproteins in the presence of AgNP of ratios 300:1 and 600:1 as measured by CD. The α-helical content is reduced with greater apolipoprotein concentration, while the β sheet content is increased. (B) Dependence of α-helical content from the GPU-optimized coarse-grained MD simulations of 15 apolipoproteins in the presence of a citrate-coated AgNP. (C) The interaction frequency of the amino acids during the simulation after 500,000 timesteps. The residues are listed in increasing order of hydrophobicity. (D) The distances between the center of mass of each of the 15 apolipoproteins and the AgNP.

AUTHOR INFORMATION

Corresponding Authors

*(S.S.C.) E-mail: choss@wfu.edu. Tel: 336-923-8370.
*(P.C.K.) E-mail: pcke11@clemson.edu.

Notes

The authors declare no competing financial interest.

ACKNOWLEDGMENTS

This work was supported by the National Science Foundation (CBET-1232724) to P.C.K. and S.S.C. S.S.C. acknowledges computational support from the Wake Forest University DEAC Cluster, where the MD simulations were performed. S.S.C. and R.L. acknowledge financial support from the Wake Forest University Center for Molecular and Cellular Communication.

REFERENCES

(1) Colvin, V. L. The Potential Environmental Impact of Engineered Nanomaterials. *Nat. Biotechnol.* **2003**, *21*, 1166−1170.

(2) Lynch, I.; Dawson, K. A.; Linse, S. Detecting Cryptic Epitopes Created by Nanoparticles. *Sci. STKE* **2006**, *2006*, pe14.

(3) Cedervall, T.; Lynch, I.; Lindman, S.; Berggård, T.; Thulin, E.; Nilsson, H.; Dawson, K. A.; Linse, S. Understanding the Nanoparticle−protein Corona Using Methods to Quantify Exchange Rates and Affinities of Proteins for Nanoparticles. *Proc. Natl. Acad. Sci. U.S.A.* **2007**, *104*, 2050−2055.

(4) Li, Y.; Budamagunta, M. S.; Luo, J.; Xiao, W.; Voss, J. C.; Lam, K. S. Probing of the Assembly Structure and Dynamics Within Nanoparticles During Interaction with Blood Proteins. *ACS Nano* **2012**, *6*, 9485−9495.

(5) Monopoli, M. P.; Åberg, C.; Salvati, A.; Dawson, K. A. Biomolecular Coronas Provide the Biological Identity of Nanosized Materials. *Nat. Nano* **2012**, *7*, 779−786.

(6) Lundqvist, M.; Stigler, J.; Cedervall, T.; Berggård, T.; Flanagan, M. B.; Lynch, I.; Elia, G.; Dawson, K. The Evolution of the Protein Corona Around Nanoparticles: A Test Study. *ACS Nano* **2011**, *5*, 7503−7509.

(7) Wang, F.; Yu, L.; Salvati, A.; Dawson, K. A. The Biomolecular Corona Is Retained During Nanoparticle Uptake and Protects the Cells from the Damage Induced by Cationic Nanoparticles Until Degraded in the Lysosomes. *Nanomed.: Nanotechnol., Biol. Med.* **2013**, in press.

(8) Salvati, A.; Pitek, A. S.; Monopoli, M. P.; Prapainop, K.; Bombelli, F. B.; Hristov, D. R.; Kelly, P. M.; Åberg, C.; Mahon, E.; Dawson, K. A. Transferrin-Functionalized Nanoparticles Lose Their Targeting Capabilities When a Biomolecule Corona Adsorbs on the Surface. *Nat. Nano* **2013**, *8*, 137−143.

(9) Anfinsen, C. B. Principles That Govern the Folding of Protein Chains. *Science* **1973**, *181*, 223−230.

(10) Bryngelson, J. D.; Wolynes, P. G. Spin Glasses and the Statistical Mechanics of Protein Folding. *Proc. Natl. Acad. Sci. U.S.A.* **1987**, *84*, 7524−7528.

(11) Bryngelson, J. D.; Onuchic, J. N.; Socci, N. D.; Wolynes, P. G. Funnels, Pathways, and the Energy Landscape of Protein Folding: a Synthesis. *Proteins* **1995**, *21*, 167−195.

(12) Leopold, P. E.; Montal, M.; Onuchic, J. N. Protein Folding Funnels: a Kinetic Approach to the Sequence-Structure Relationship. *Proc. Natl. Acad. Sci. U.S.A.* **1992**, *89*, 8721−8725.

(13) Onuchic, J. N.; Wolynes, P. G. Theory of Protein Folding. *Curr. Opin. Struct. Biol.* **2004**, *14*, 70−75.
(14) Levy, Y.; Cho, S. S.; Onuchic, J. N.; Wolynes, P. G. A Survey of Flexible Protein Binding Mechanisms and Their Transition States Using Native Topology Based Energy Landscapes. *J. Mol. Biol.* **2005**, *346*, 1121−1145.
(15) Shea, J. E.; Brooks, C. L. From Folding Theories to Folding Proteins: a Review and Assessment of Simulation Studies of Protein Folding and Unfolding. *Annu. Rev. Phys. Chem.* **2001**, *52*, 499−535.
(16) Dill, K. A.; Bromberg, S.; Yue, K.; Fiebig, K. M.; Yee, D. P.; Thomas, P. D.; Chan, H. S. Principles of Protein Folding: a Perspective from Simple Exact Models. *Protein Sci.* **1995**, *4*, 561−602.
(17) Clementi, C.; Nymeyer, H.; Onuchic, J. N. Topological and Energetic Factors: What Determines the Structural Details of the Transition State Ensemble and "En-route" Intermediates for Protein Folding? An Investigation for Small Globular Proteins. *J. Mol. Biol.* **2000**, *298*, 937−953.
(18) Hills, R. D.; Brooks, C. L. Insights from Coarse-Grained Gō Models for Protein Folding and Dynamics. *Int. J. Mol. Sci.* **2009**, *10*, 889−905.
(19) Cho, S. S.; Levy, Y.; Wolynes, P. G. Quantitative Criteria for Native Energetic Heterogeneity Influences in the Prediction of Protein Folding Kinetics. *Proc. Natl. Acad. Sci. U.S.A.* **2009**, *106*, 434−439.
(20) Karanicolas, J.; Brooks, C. L. The Origins of Asymmetry in the Folding Transition States of Protein L and Protein G. *Protein Sci.* **2002**, *11*, 2351−2361.
(21) Ejtehadi, M. R.; Avall, S. P.; Plotkin, S. S. Three-Body Interactions Improve the Prediction of Rate and Mechanism in Protein Folding Models. *Proc. Natl. Acad. Sci. U.S.A.* **2004**, *101*, 15088−15093.
(22) Thirumalai, D.; Hyeon, C. RNA and Protein Folding: Common Themes and Variations. *Biochemistry* **2005**, *44*, 4957−4970.
(23) Cho, S. S.; Pincus, D. L.; Thirumalai, D. Assembly Mechanisms of RNA Pseudoknots Are Determined by the Stabilities of Constituent Secondary Structures. *Proc. Natl. Acad. Sci. U.S.A.* **2009**, *106*, 17349−17354.
(24) Hyeon, C.; Thirumalai, D. Capturing the Essence of Folding and Functions of Biomolecules Using Coarse-Grained Models. *Nat. Commun.* **2011**, *2*, 487.
(25) Bailor, M. H.; Mustoe, A. M.; Brooks, C. L., III; Al-Hashimi, H. M. Topological Constraints: Using RNA Secondary Structure to Model 3D Conformation, Folding Pathways, and Dynamic Adaptation. *Curr. Opin. Struct. Biol.* **2011**, *21*, 296−305.
(26) Cheung, M. S.; Klimov, D.; Thirumalai, D. Molecular Crowding Enhances Native State Stability and Refolding Rates of Globular Proteins. *Proc. Natl. Acad. Sci. U.S.A.* **2005**, *102*, 4753−4758.
(27) Morriss-Andrews, A.; Shea, J.-E. Kinetic Pathways to Peptide Aggregation on Surfaces: The Effects of B-Sheet Propensity and Surface Attraction. *J. Chem. Phys.* **2012**, *136*, 065103−065111.
(28) Morriss-Andrews, A.; Bellesia, G.; Shea, J.-E. B-Sheet Propensity Controls the Kinetic Pathways and Morphologies of Seeded Peptide Aggregation. *J. Chem. Phys.* **2012**, *137*, 145104−145109.
(29) Vilaseca, P.; Dawson, K. A.; Franzese, G. Understanding and Modulating the Competitive Surface-Adsorption of Proteins through Coarse-Grained Molecular Dynamics Simulations. *Soft Matter* **2013**, *9*, 6978−6985.
(30) Zannis, V. I.; Chroni, A.; Krieger, M. Role of apoA-I, ABCA1, LCAT, and SR-BI in the Biogenesis of HDL. *J. Mol. Med* **2006**, *84*, 276−294.
(31) Dagher, G.; Donne, N.; Klein, C.; Ferré, P.; Dugail, I. HDL-mediated Cholesterol Uptake and Targeting to Lipid Droplets in Adipocytes. *J. Lipid Res.* **2003**, *44*, 1811−1820.
(32) Pincus, D. L.; Cho, S. S.; Hyeon, C.; Thirumalai, D. Minimal Models for Proteins and RNA from Folding to Function. *Prog. Mol. Biol. Transl. Sci.* **2008**, *84*, 203−250.
(33) Cho, S. S.; Levy, Y.; Wolynes, P. G. P Versus Q: Structural Reaction Coordinates Capture Protein Folding on Smooth Landscapes. *Proc. Natl. Acad. Sci. U.S.A.* **2006**, *103*, 586−591.
(34) Kumar, S.; Bouzida, D.; Swendsen, R. H.; Kollman, P. A.; Rosenberg, J. M. The Weighted Histogram Analysis Method for Free-Energy Calculations on Biomolecules 0.1. The Method. *J. Comput. Chem.* **1992**, *13*, 1011−1021.
(35) Lipscomb, T. J.; Zou, A.; Cho, S. S. Parallel Verlet Neighbor List Algorithm for GPU-optimized MD Simulations. In *Proceedings of the ACM Conference on Bioinformatics, Computational Biology and Biomedicine*; BCB '12; ACM: New York, 2012; pp 321−328.
(36) Proctor, A. J.; Lipscomb, T. J.; Zou, A.; Anderson, J. A.; Cho, S. S. GPU-Optimized Coarse-Grained MD Simulations of Protein and RNA Folding and Assembly. *Science J.* **2012**, *1*, 1−11.
(37) Cho, S. S.; Weinkam, P.; Wolynes, P. G. Origins of Barriers and Barrierless Folding in BBL. *Proc. Natl. Acad. Sci. U.S.A.* **2008**, *105*, 118−123.
(38) Biyun, S.; Cho, S. S.; Thirumalai, D. Folding of Human Telomerase RNA Pseudoknot Using Ion-Jump and Temperature-Quench Simulations. *J. Am. Chem. Soc.* **2011**, *133*, 20634−20643.
(39) Veitshans, T.; Klimov, D.; Thirumalai, D. Protein Folding Kinetics: Timescales, Pathways and Energy Landscapes in Terms of Sequence-dependent Properties. *Folding Des.* **1997**, *2*, 1−22.
(40) Shen, X.-C.; Liou, X.-Y.; Ye, L.-P.; Liang, H.; Wang, Z.-Y. Spectroscopic Studies on the Interaction Between Human Hemoglobin and CdS Quantum Dots. *J. Colloid Interface Sci.* **2007**, *311*, 400−406.
(41) Kaufman, E. D.; Belyea, J.; Johnson, M. C.; Nicholson, Z. M.; Ricks, J. L.; Shah, P. K.; Bayless, M.; Pettersson, T.; Feldotö, Z.; Blomberg, E.; et al. Probing Protein Adsorption onto Mercaptoundecanoic Acid Stabilized Gold Nanoparticles and Surfaces by Quartz Crystal Microbalance and ζ-Potential Measurements. *Langmuir* **2007**, *23*, 6053−6062.
(42) Darabi Sahneh, F.; Scoglio, C.; Riviere, J. Dynamics of Nanoparticle−Protein Corona Complex Formation: Analytical Results from Population Balance Equations. *PLoS One* **2013**, *8*, e64690.